9-2002

An east Asian cold surge: Case study

Tsing-Chang Chen
Iowa State University, tmchen@iastate.edu

Ming-Cheng Yen
National Central University

Wan-Ru Huang
Iowa State University

William A. Gallus Jr.
Iowa State University, wgallus@iastate.edu

An East Asian Cold Surge: Case Study

TSING-CHANG CHEN

Atmospheric Science Program, Department of Geological and Atmospheric Sciences, Iowa State University, Ames, Iowa

MING-CHENG YEN

Department of Atmospheric Science, National Central University, Chung-Li, Taiwan

WAN-RU HUANG AND WILLIAM A. GALLUS JR.

Atmospheric Science Program, Department of Geological and Atmospheric Sciences, Iowa State University, Ames, Iowa

(Manuscript received 15 June 2001, in final form 5 March 2002)

ABSTRACT

Since a cold surge is a hazardous weather phenomenon in east Asia, the rapid population increase and economic growth over the past two decades require improvement in forecasting cold surges and their related weather events over this region. However, without a better understanding of these events, this task cannot be accomplished. A cold surge with a well-defined cold front passing through Taiwan was selected to illustrate its impact on the east Asian weather system. This case is typical of a large portion of surges occurring in the region. Major findings of this study are as follows. Coupling with the upper ridge–trough structures of the wave train straddling the eastern seaboard of northeast Asia, cold surges occur sequentially. A cold front with a prefront high pressure zone is formed by the new surge outflow interacting with the anticyclone of the aging surge. The warm moist air advected northeastward along the cold front assists the development of the new surge's low center, while the prefront high pressure zone facilitates the formation of a double-cell structure in the local Hadley circulation. The southeastward propagation of the cold front is driven by the eastward-propagating short-wave trough through the couplets of both new and aging cold surges. The surface weather conditions in the low-elevation zones of Taiwan are modulated by the cold surge flow, but the high-elevation areas may be affected instead by the tropical southeast Asian high. Despite the success of the prior and post-WMONEX (Winter Monsoon Experiment) research in exploring the tropical–midlatitude interaction, the close interaction of cold surges with local weather systems and the planetary-scale circulation in east Asia, illustrated by the case study presented, provides another dimension of cold surge research.

1. Introduction

Cold surges, hazardous weather phenomena in east–southeast Asia (Ramage 1971), were not systematically studied until the Winter Monsoon Experiment (WMONEX; Greenfield and Krishnamurti 1979). A summary of prior and post-WMONEX research of cold surges, especially the tropical–midlatitude interaction, was given in a comprehensive review by Lau and Chang (1987). Some major findings pertaining to the present study are given in brief.

a. Surface conditions

The arrival of a cold surge is generally characterized by a steep rise of surface pressure (p_s), a sharp drop of surface temperature (T_s), and a strengthening of northerly surface winds (v_s). Through further analysis of surface synoptic conditions, Chang et al. (1983) observed that the surge arrival may consist of two steps: the edge passage of the high-density cold-air current reflected by a drastic increase in p_s, and the thermal frontal passage indicated by a sharp drop in dewpoint (T_d). The separation time between these two steps becomes large in tropical areas downstream.

b. Synoptic environment

The onset of an east Asian cold surge follows the establishment of northwesterly flow via a ridge aloft over Lake Baikal. A short-wave trough ahead of this ridge deepens as it propagates across the eastern seaboard of northeast Asia. This upper-air ridge–trough structure induces the southward surface cold-air outbreak from the eastern Siberian high. The cold surge flow forms an anticyclone–cyclone couplet with a high

Corresponding author address: Professor Tsing-Chang (Mike) Chen, Atmospheric Science Program, Department of Geological and Atmospheric Sciences, Iowa State University, 3010 Agronomy Hall, Ames, IA 50011.
E-mail: tmchen@iastate.edu.

pressure center over continental east Asia and a low pressure center over Japan (Lau and Lau 1984).

c. Tropical–midlatitude interaction

The local Hadley circulation of the southeast Asian longitudes is intensified by tropical convection following cold surges. The tropical–midlatitude interaction therefore is established by the local Hadley circulation through the Coriolis acceleration associated with the upper southerly branch, which speeds up the east Asian jet (Chang and Lau 1980, and others).

Two implicit simplifications were adopted in these findings: (a) the interaction between the cold surge and planetary-scale circulation is illustrated conceptually with a single cold surge model, and (b) there is no active interaction between the cold surge flow and the east Asian weather. These simplifications lead us to the following questions.

- As revealed from lower-tropospheric streamline charts, some east Asian cold surges may form *sequentially*. How does the presence of an aging cold surge downstream affect the development of a subsequent surge upstream?
- The tropical southeast Asian high at upper levels was generally ignored in the WMONEX research. How does this high influence the regional winter weather in east Asia?
- A cold surge's arrival is characterized by a sharp p_s rise, a sudden T_s drop, and a drastic increase of northerly/northeasterly wind. What may be the cold surge impact on the regional weather conditions beyond this characterization?

Cold surges during the 11 winters (December–February) of 1989–2000 were identified with three slightly modified criteria of Lau and Chang (1987) plus an additional synoptic condition. Surface observations at the Pengehiayu station (~20 km northeast of Keelung, the largest seaport of northern Taiwan) exhibit the following changes within 24 ~ 48 h: (a) surface pressure (p_s) increases $\geq$5 mb, (b) surface temperature drops $\geq$4°C, (c) surface prevailing wind is $\geq$3 m s^{-1}, and (d) the cold surge outflow over east Asia can be clearly identified by the Geostationary Meteorological Satellite (GMS) infrared (IR)/visible images and 925-mb streamline charts. Ninety-three cold surges were identified; fifty-two of them (56%) exhibit double surge couplets with their synoptic conditions similar to those revealed from composite streamline charts presented by Lau and Lau (1984) at 500 mb (their Fig. 3b) and 1000 mb (their Fig. 4). Since the composite procedure may smooth some synoptic details, we select one of 52 cases for an in-depth analysis to explore the three aforementioned questions. The selected case exhibits not only the synoptic conditions common to the other 51 cold surges, but also some interesting cloud images described later.

Four cloud images of this cold surge observed by the Geostationary Meteorological Satellite are shown in Fig. 1. The frontal passage across Taiwan is highly visible during 7–8 January 1996. Based upon the IR (before sunrise) and visible (VIS; after sunrise) images (each hour) and surface charts issued by the Japan Meteorological Agency (every 6 h), the cold surge front location every hour is depicted by solid lines in Fig. 2. Even though Taiwan is small in size (~30 000 km^2; the north–south extent is about 400 km, and its maximum east–west width is about 150 km), it has complex orography and is geographically divided by a north–south-oriented central mountain range into the western low plains and the eastern valley and coastal terrain. The tallest mountain of this island, Yushan, reaches an elevation close to 4000 m. However, as revealed from Fig. 1, the tall mountains are free of clouds. Therefore, the clouds associated with the cold surge front must have crept around these mountains. It will be shown later that this interesting feature of the cold surge front may not be completely attributed to the shallow depth of the surge. As inferred from cloud images in Fig. 1, this cold surge likely affected surface weather conditions significantly over Taiwan and east Asia.

Three data sources are used in this analysis; GMS observations, National Centers for Environmental Prediction–National Center for Atmospheric Research (NCEP–NCAR) reanalysis data (Kalnay et al. 1996), and surface observations from Taiwan stations. The GMS IR and visible data used in this study were provided by the Center for Space and Remote Sensing Research in Taiwan with resolutions of 5 km × 5 km and 1.25 km × 1.25 km, respectively. The resolution of the NCEP–NCAR reanalysis is 2.5° × 2.5°, which may not be sufficient to portray the detailed structure of some mesoscale systems but the depiction of these systems is verified with the GMS IR and visible images. Surface observations around Taiwan are routinely recorded every hour by 25 stations (shown later in section 5) administrated by the weather bureau of Taiwan. The entire study is arranged in the following manner: the synoptic environment, including upper troposphere, surface, and local Hadley circulations, are analyzed in sections 2, 3, and 4, respectively. The impact of this cold surge on surface weather conditions in Taiwan is presented in section 5. Some concluding remarks are offered in section 6.

2. Upper-air synoptic environment

At 1200 UTC on 7 January 1996, a well-organized cold surge couplet (H_1/L_1) existed east of Japan and west of the eastern subtropical Pacific anticyclone (Fig. 3e). This couplet connected with an upper-level shortwave ridge–trough (R_1/T_1) system (Fig. 3a) with a ridge (R_1) line along Japan and a cutoff low (T_1) east of the Kuril Islands. The synoptic conditions resembled the composite conditions of 11 WMONEX east Asian cold-air outbreaks compiled by Lau and Lau (1984; their

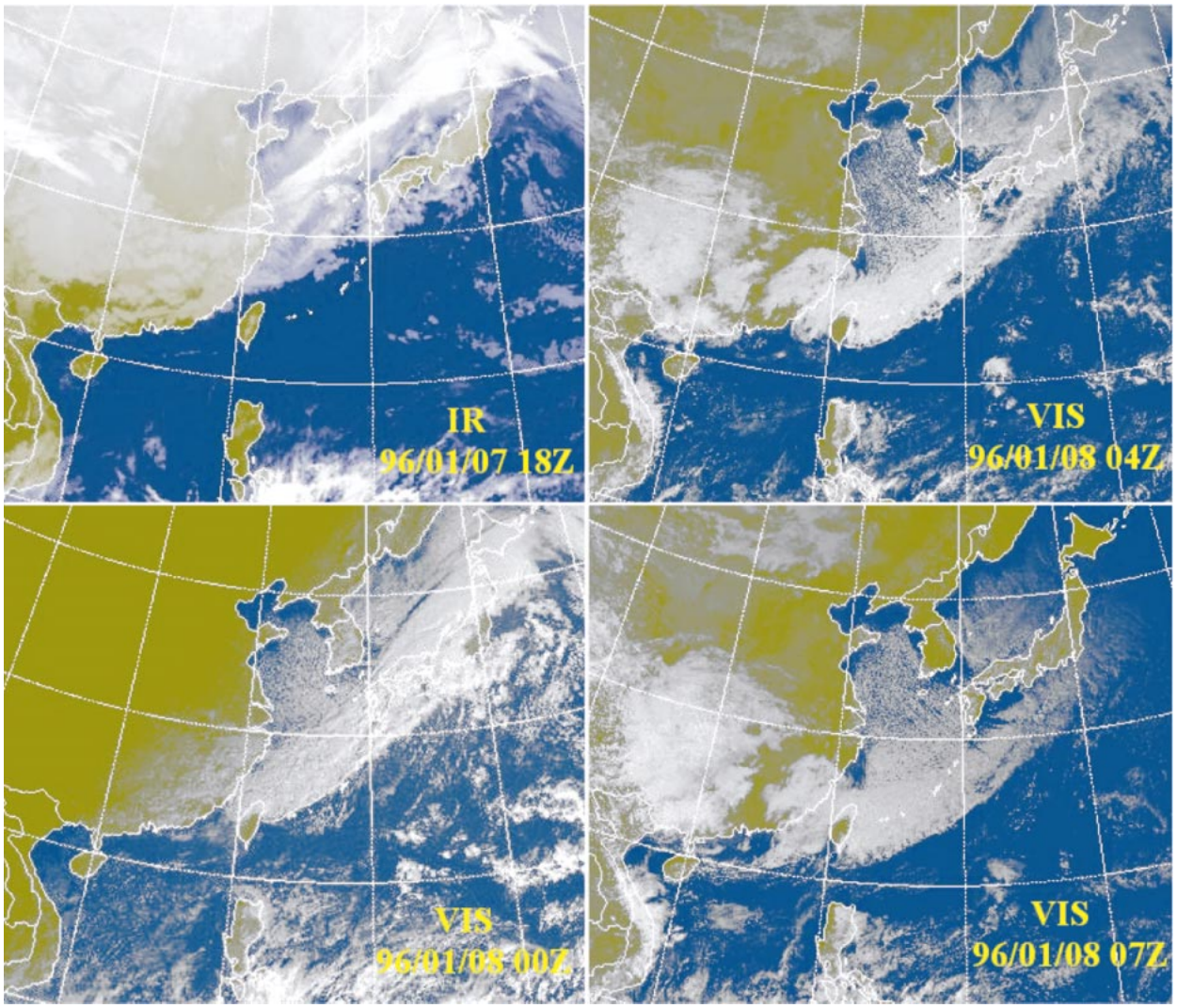

FIG. 1. Cloud images (white color) observed by the IR and VIS channels of the GMS of Japan at times indicated in each lower-right corner.

Figs. 3b and 4). West of the oceanic ridge–trough system appeared another continental ridge–trough (R_2/T_2) system, which consisted of a broad Lake Baikal ridge (R_2) and a short-wave trough (T_2) adjacent to the eastern seaboard of northeast Asia. Behind the oceanic cold surge couplet, the low-level continental synoptic conditions were dominated by an anticyclone south of Lake Baikal and a trough along the east Asian coast. Twelve hours later at 0000 UTC on 8 January (Fig. 3f), a second cold surge couplet (H_2/L_2) emerged along the eastern seaboard with a continental surface high (H_2) over east Asia and a surface low (L_2) centered over the northern Japan Sea (Fig. 3f), Like the oceanic cold surge couplet, this continental couplet also connected with the continental short-wave trough–ridge structure (Fig. 3b). The cold surge advancing across Taiwan toward Southeast Asia merges with the northeasterlies of this couplet's anticyclonic cell (H_2). Thus, the upper-level synoptic conditions, particularly the appearance of the Lake Baikal ridge, have been used operationally by the Hong Kong Observatory as the precursor of an imminent cold surge.

Despite the resemblance of the synoptic environment associated with the cold surge analyzed in the current study with Lau and Lau's (1984) composite WMONEX case, several interesting features of the present cold surge synoptic environment have not been previously documented. A SW–NE-oriented perturbation train was formed by the continental cold surge couplet (H_2/L_2; Fig. 3f) with a disturbance over eastern Siberia. Parallel to this perturbation train was another one formed by the oceanic couplet (H_1/L_1). Previous studies focused primarily on the continental cold surge couplet. Actually, the cold surge couplets are generated sequentially over east Asia and the northwest Pacific. The composite WMONEX cold surge couplet of Lau and Lau (1984)

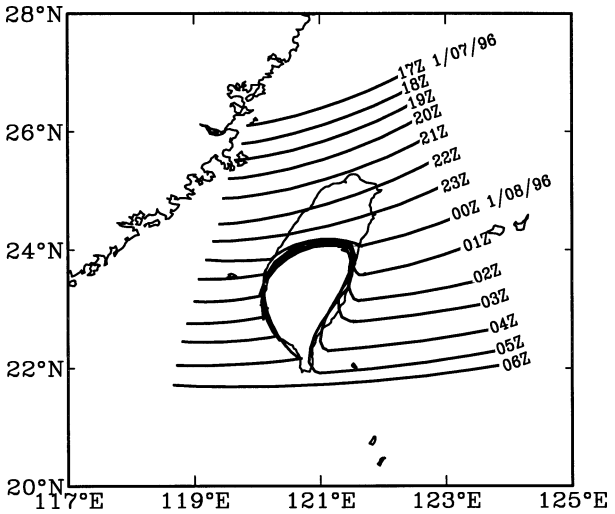

FIG. 2. Locations of the cold surge front identified with the GMS IR/VIS cloud images, surface analysis charts issued by the JMA, and surface streamline charts constructed with the NCEP–NCAR reanalysis data.

propagated northeastward, while both couplets shown in Fig. 3 propagated *eastward.* Because of the coupling between the cold surge couplet and the upper-level short-wave ridge–trough structure, the propagation property of the cold surge couplet is essentially determined by that of the upper-level short wave. Compiling all cold surge couplets over the past 11 winters (1989–2000), we found that the populations of both propagation tracks are roughly comparable (about 50% to 50%).

An interesting research aspect of the east Asian cold surge pursued by previous studies was to examine the propagation and structure of cold surge disturbances in relation to the downstream development of synoptic disturbances in midlatitudes (Joung and Hitchman 1982; Lau and Lau 1984; Chang 1993; Orlanski and Chang 1993). As shown in Figs. 3e–h, the southwestward flow of the oceanic couplet's anticyclonic cell (H_1) may generate cold surge vortices not only over the tropical South China Sea, but also over the tropical Philippine Sea. The possible impact of the aging oceanic cold surge couplet (H_1/L_1) on the tropical circulation was not noticed until recently. Based upon observations and numerical simulations, Palmer and Owen (1986) and Moore et al. (2000) suggested that a possible teleconnection link may exist between the tropical western Pacific and North America. This teleconnection link was shown recently by Chen (2002) through a North Pacific teleconnection short-wave train induced by the anomalous western tropical Pacific forcing, which is generated by the interannual variation in the occurrence of the aforementioned cold surge vortices in the Tropics.

As shown in Figs. 3a–d, the eastward propagation of the short-wave trough along the eastern seaboard is accompanied by a coherent propagation of the tropical southeast Asian high (H). To support our observation, the longitude–time (x–t) diagrams of 300-mb streamfunction and ψ(300 mb) at 20°N and 45°N are displayed in Fig. 4. The Baikal ridge and the east coast trough are denoted by R_2 and T_2, respectively, in Fig. 4b, while the southeast Asian high is marked by H in Fig. 4a. Coherent eastward propagation of the east coast trough and the southeast Asian high is indicated by parallel strips of ψ(300 mb) anomalies at 20°N (marked by H) and 45°N (marked by T_2). Another interesting feature between these two circulation components is the *deepening* of the east coast trough followed by the *amplification* of the southeast Asian high. It was concluded by a number of previous studies [reviewed by Lau and Chang (1987)] that the east Asian cold surge enhances tropical convection, and in turn intensifies the local Hadley circulation. The east Asian jet is then accelerated by the upper southerly branch of this circulation through the Coriolis force. Since zonal wind speed is determined by the meridional gradient of streamfunction, the intensification of the east Asian jet (indicated by stippled areas in Figs. 3a–d) should be a result of the synchronous evolution of the east coast trough and the southeast Asian high. Thus, the intensification of the east Asian jet during a cold surge may be explained in a different perspective with the development of the synoptic relationship between this high and the east coast trough. A quantitative analysis to clarify this argument and the southeast Asian high's evolution observed by a surface station at Yushan in Taiwan will be presented in section 5.

3. Surface synoptic conditions

The surface weather charts issued by the Japan Meteorological Agency (JMA) for 7–9 January 1996 are shown in Fig. 5. The lower-tropospheric synoptic conditions of the cold surge in Figs. 3e–h are characterized by a continental and an oceanic cold surge couplet over the northwest Pacific and are well reflected by the corresponding surface high (low) pressure centers in Fig. 5. Some interesting features unique to the synoptic conditions and vital to the development of the weather system associated with the east Asian cold surge may not be noticeable in the upper-air charts, but are revealed from surface weather charts.

A ''prefront trough'' often appears ahead of a well-

→

FIG. 3. Streamline charts for (a–d) 300 mb and (e–h) 850 mb for four synoptic times indicated in each upper-left corner. Troughs and ridges at 300 mb are marked by (T_1, T_2, R_1, R_2), while high and low centers at 850 mb are denoted by (H_1, H_2, L_1, L_2). Isotachs within the ranges shown in each lower-right corner are colored light and dark gray.

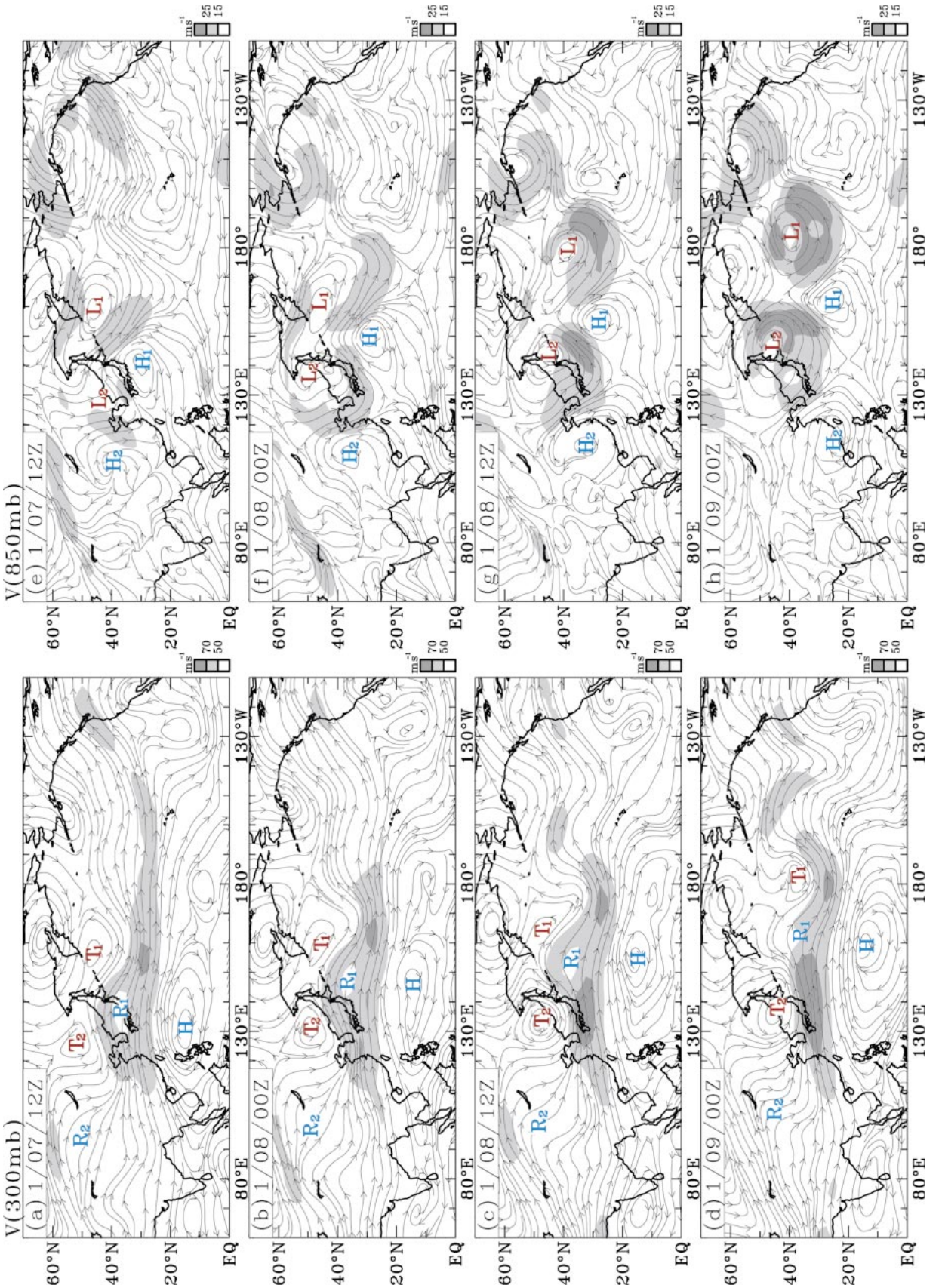
V(300mb)
V(850mb)
(a) 1/07/12Z
(b) 1/08/00Z
(c) 1/08/12Z
(d) 1/09/00Z
(e) 1/07/12Z
(f) 1/08/00Z
(g) 1/08/12Z
(h) 1/09/00Z
60°N
40°N
20°N
EQ
80°E
130°E
180°
130°W
ms-1
70
50
25
15
T1
T2
R1
R2
H
L1
L2
H1
H2

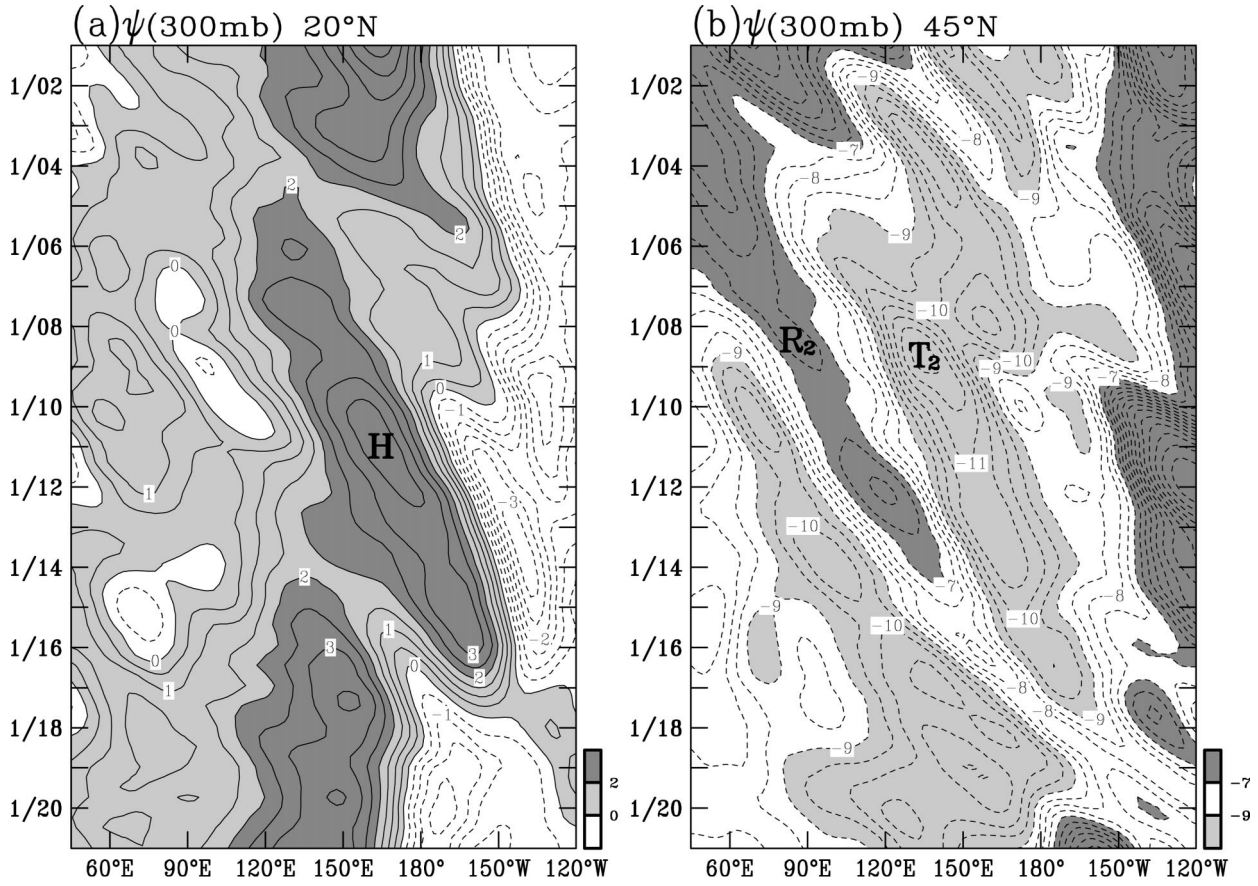

FIG. 4. Longitude (x)–time (t) diagrams of 300-mb streamfunction ψ(300 mb) at (a) 20°N and (b) 45°N; values of ψ(300 mb) ≥ 0 and $\geq 2 \times 10^7$ m^2 s^{-1} at 20°N are lightly and heavily stippled respectively, while for 45°N those values $\geq -7 \times 10^7$ m^2 s^{-1} and $\leq -9 \times 10^7$ m^2 s^{-1} are heavily and lightly stippled respectively. The contour interval of ψ(300 mb) is 5×10^6 m^2 s^{-1}.

developed cold front associated with southward movement of cold anticyclones in the southern plains of North America (e.g., Locatelli et al. 1998; Clarke 1998; Blustein 1993); surface wind directions shift from south or southeast to southwest or west across this trough. For the cold front associated with the east Asian cold-air outbreak, the weather conditions around this front generally differ from those around the North American cold front. Instead of a prefront trough, a high pressure zone (which will be illustrated further in Fig. 6) often exists ahead of the east Asian cold front. As shown in Fig. 5, this prefront high pressure zone seems to be formed by the westward extension of the anticyclonic cell (H_1 in Figs. 3e–h) of the oceanic couplet. Thus, surface wind directions exhibit no significant change across the cold front, except for a small-scale perturbation in the vicinity of Taiwan. This observation will be confirmed later by station observations in Taiwan. The east–west broadly stretched prefrontal high pressure zone may exert a blocking effect on the cold surge outflow to form the continental cold surge couplet (H_1/L_1 in Figs. 3e–h). It becomes clear at this point that the anticyclonic cell (H_1 in Figs. 3e–f) of this oceanic couplet is not only remotely involved in the genesis of cold surge vortices in the tropical Philippine and South China Seas (indicated by streamlines in Figs. 3e–h), but can also affect the development of the continental cold surge couplet (H_2/L_2) over the eastern seaboard of east Asia.

The interaction between the oceanic and continental cold surge couplets is illustrated further in terms of the p_s fields (derived from the NCEP reanalysis data) shown in Fig. 6. It is revealed from the region of $p_s \geq 1020$ mb at 0000 UTC 7 January 1996 (Fig. 6a) that the cold-air outbreak of the oceanic couplet covered the northwest Pacific–east Asian region. Behind this cold-air mass, another cold-air outbreak started to form over north-northwest China (indicated by $p_s \geq 1028$ mb and streamlines converging southward). Twelve hours later, the newly developed continental cold-air outbreak intensified and advanced further southward. Consequently, the weakening oceanic high (of the oceanic couplet) and the growing continental cold-air outbreak (of the continental couplet) are bridged together to establish a high pressure zone along the cold front. By 0000 UTC 8 January, this high pressure zone [indicated by the region of $p_s \geq 1020$ mb (reanalysis data) in Fig. 6c and

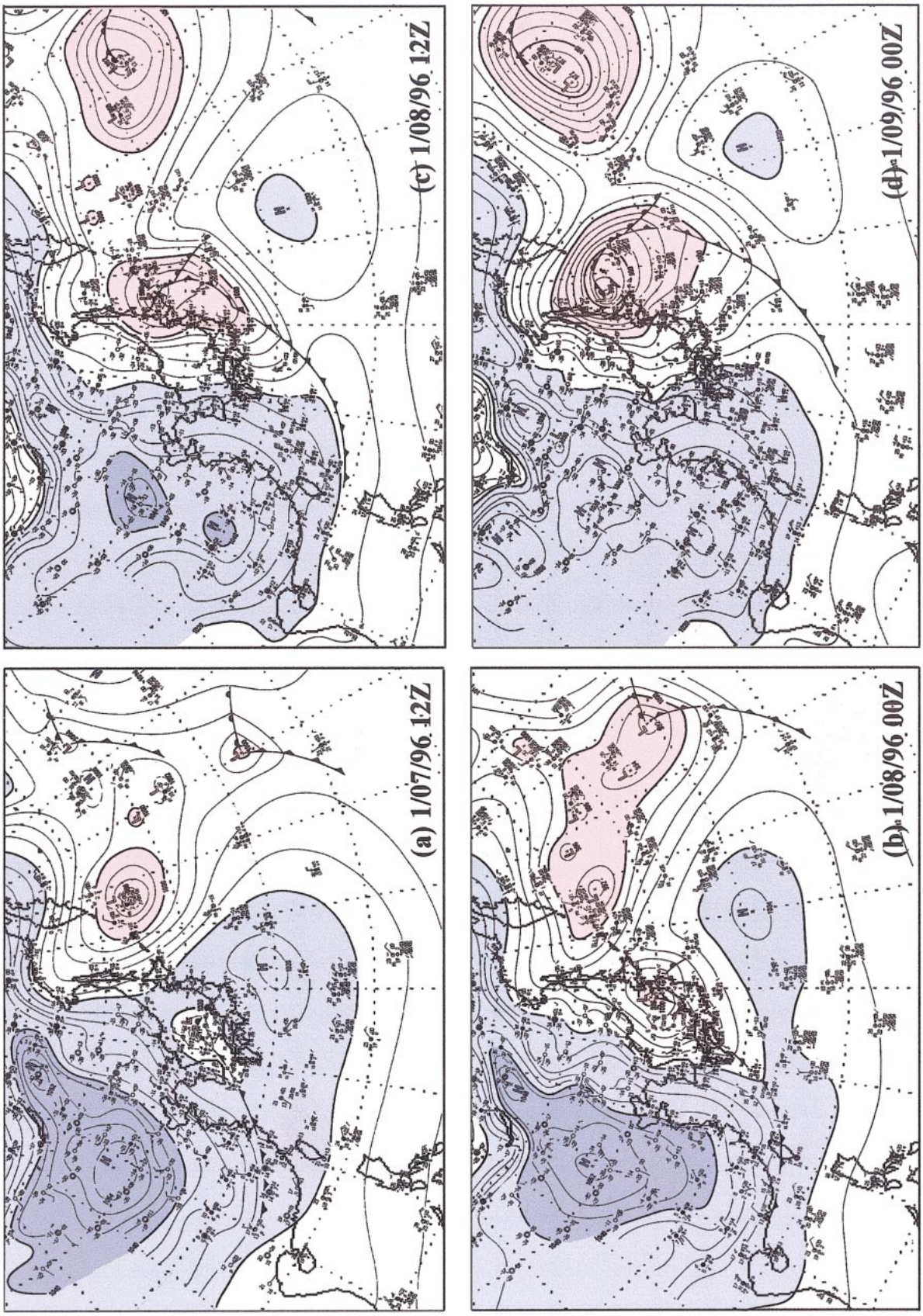

FIG. 5. Surface analyses at four synoptic times (indicated in the lower-right corner) issued by the JMA. Values of $p_s \geq 1040$ mb, $1040 \text{ mb} \geq p_s \geq 1020$ mb, and $1000 \text{ mb} \geq p_s$ are colored blue, light blue, and pink, respectively.

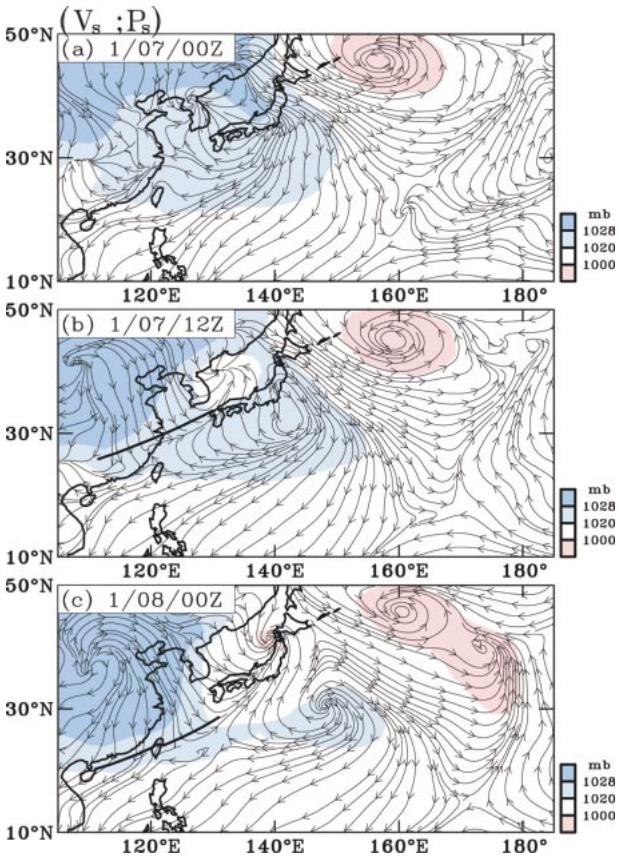

FIG. 6. Surface streamline (V_s) charts with p_s at three synoptic times (indicated in the upper-left corner); the cold surge front is indicated by a thick dark line, while values of $p_s \geq 1028$ mb, 1028 mb $\geq p_s \geq$ 1020 mb, and 1000 mb $\geq p_s$ are colored blue, light blue, and pink, respectively.

enclosed by the 1020-mb contour in Fig. 5b (JMA observations)] narrowed and stretched eastward following the eastward propagation of the ocean high center.

The interaction between the continental and oceanic couplets presented earlier may exert some dynamic impact on the east Asian surface weather conditions. Along this line, three examples are presented in the following:

a. The meteorological conditions around the cold front

Note that the cold front was located in central Taiwan at 0000 UTC 8 January 1996. We shall focus our analysis for the possible effect of the aforementioned interaction on the meteorological conditions around the cold front at this particular synoptic time (Fig. 7). The convergence of the southward intrusive cold air toward the prefront high pressure may result in an upward motion zone along the cold front (Fig. 7a). In addition, the warm-air advection along the cold front (Fig. 7b) by the northeastward confluent flows formed by the H_1 anticyclonic flow and the L_2 cyclonic flow helps to maintain the moist (large-value W) frontal zone (Fig. 7d) and facilitates the development of a downstream low center located over northern Japan. Because of its low temperature, the intrusive cold surge outflow moving over the warm sea surface forms a convectively unstable inversion layer behind the front (indicated by the skew T–log$p$ chart of the Taipei radiosonde observation at 0000 UTC 8 January in Fig. 8). Consequently, the dewpoint depression ΔT_d(925 mb)[$=T$(925 mb) $- T_d$(925 mb), T_d(925 mb) is dewpoint at 925 mb] was low over the ocean behind the front (Fig. 7c). As indicated by P_{GPI} [Goddard precipitation estimate by Susskind et al. (1997)] (Fig. 7e) and $\Delta T_{\text{BB}}[=T_{\text{BB}} - \overline{T}_{\text{BB}}$; T_{BB} is equivalent blackbody temperature observed by GMS and $\overline{T}_{\text{BB}}$ = January-mean value of T_{BB}] (Fig. 7f), precipitation occurred behind the cold front, but did not form a wide frontal rainband like an anafront (Browning 1990). This argument is consistent with shallow-convective clouds behind the front (Fig. 1) and the rainfall measurements at different local standard times in Taiwan (Fig. 9). The lack of precipitation ahead of the cold front in the present study is likely attributed to subsidence associated with the prefront high pressure zone (which will be illustrated in section 4).

b. The southeastward advance of the cold front

The southeastward movement of the cold front shown in Fig. 2 follows the advancement of the cold-air mass (Fig. 5), but the location and movement of the cold front is determined by the interaction between two cold surge couplets. As illustrated in Fig. 3, couplets are connected with two short-wave ridge–trough structures over the eastern seaboard. Thus, the southeastward movement of the cold surge front should be coupled with the eastward propagation of the upper-level short-wave ridge–trough structure. To substantiate this argument, the chronological locations of the trough line (T_2) and locations of the cold surge front at different synoptic times are imposed on the 300 and 850 mb streamline charts at 0000 UTC 8 January 1996 in Figs. 10a and 10b, respectively. The eastward propagation of the short-wave trough and the southeastward movement of the cold front are clearly discernable. As indicated by the locations of the T_2 trough line at 45°N (dot) and the front at 30°N (solid triangle) against time (ordinate) and longitudes (abscissa) in Fig. 10c, these two components of the cold surge weather system move eastward in a coherent manner. This coherent propagation supports our aforementioned argument; the southeastward movement of the cold surge front is coupled with the eastward propagation of the short-wave trough.

c. Separation time between the density current edge and the thermal front

The sharp rise of p_s and sudden drop of T_d at a station was used by Chang et al. (1983) as criteria to determine the arrival of a cold surge. Two possible stages of the

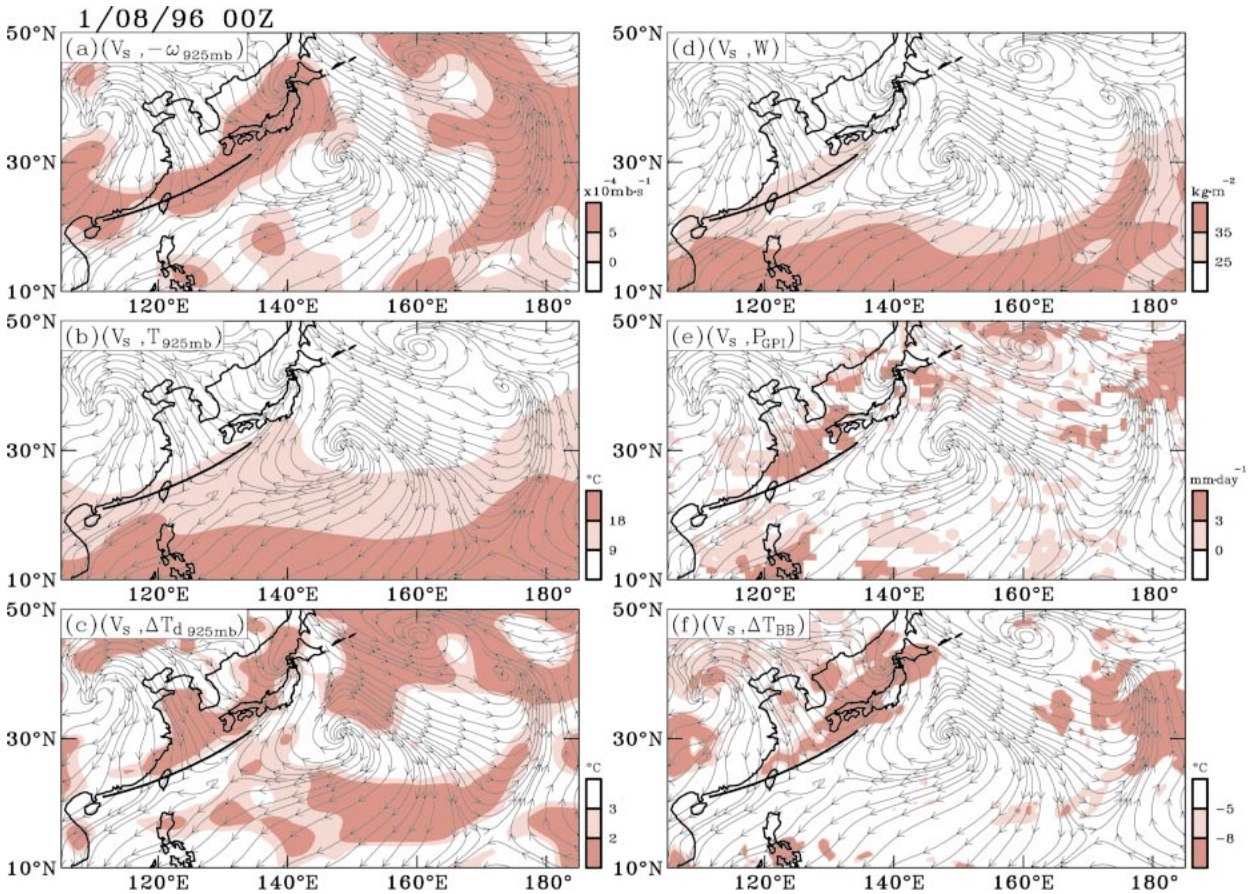

FIG. 7. Surface streamline (V_s) charts at 0000 UTC 8 Jan 1996 superimposed with the following variables: (a) $-\omega$(925 mb); (b) T(925 mb); (c) ΔT_d(925 mb)[$=T$(925 mb) $- T_d$(925 mb); (d) W (precipitable water); (e) P_{GPI}; and (f) ΔT_{BB}[$=T_{BB} - \overline{T}_{BB}$: T_{BB} is equivalent blackbody temperature and $\overline{T}_{BB}$ = January mean T_{BB}]. Values of the variables larger than those in the lower-right corner are colored pink and light pink, respectively.

cold surge arrival were identified in most of the cold surges; the advance speed of the cold-air current edge ($\sim$40 m s^{-1}) indicated by the p_s increase is much faster than the cold front movement ($\sim$11 m s^{-1}) indicated by the T_d drop. The difference of arrival time between the sharp p_s increase (the density current edge) and the sudden T_d decrease (thermal front) was defined by Chang et al. (1983) as the *separation time.* Surface observations of p_s and T_d at two stations in Taiwan [Penchiayu (the most northern station of Taiwan) and Tawu (a southeastern station of Taiwan)] separated by a distance of about 400 km are used to estimate the possible separation time. Certainly there is an arrival time difference in the thermal front between the two stations; however, based on Chang et al.'s argument, there is no separation time at both stations as determined by time series of p_s and T_d at these two stations (Fig. 11). One may argue that this nonexistence of separation time is attributed to the short distance between the two stations. As inferred from the evolution of p_s shown in Figs. 5 and 6, the arrival time of the density current edge associated with the H_2 anticyclone should be determined by the interaction between the anticyclones (H_1 and H_2) of the two couplets. In contrast, the arrival time of the thermal front seems to be affected by the eastward propagation of the upper-level short-wave ridge–trough system over the eastern seaboard (as indicated in Fig. 10). Therefore, a more accurate measurement of the separation time may have to consider the joint effect of both H_1 and H_2 anticyclones.

4. Local Hadley circulation

It was demonstrated by previous east Asian cold surge studies (reviewed by Lau and Chang 1987) that the equatorward spreading of cold air following a cold surge may enhance the tropical convective activity, and in turn intensify the local Hadley circulation in east Asia. Examining a WMONEX cold surge, Chu and Park (1984) suggested that this local Hadley circulation possibly possesses a double-cell structure separated by a downward branch over the northern part of the South China Sea. In midlatitudes, the upward (downward) motion exists ahead of a trough (ridge). Thus, an upper-(lower)

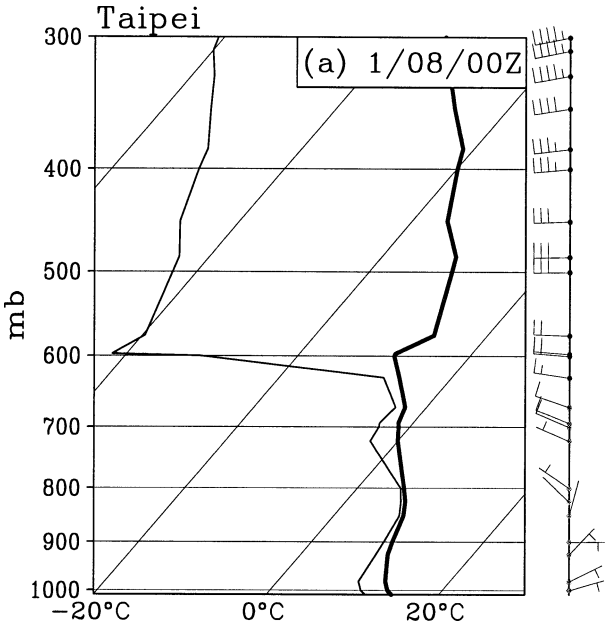

FIG. 8. A skew *T* analysis from Taipei at 0000 UTC 8 Jan 1996.

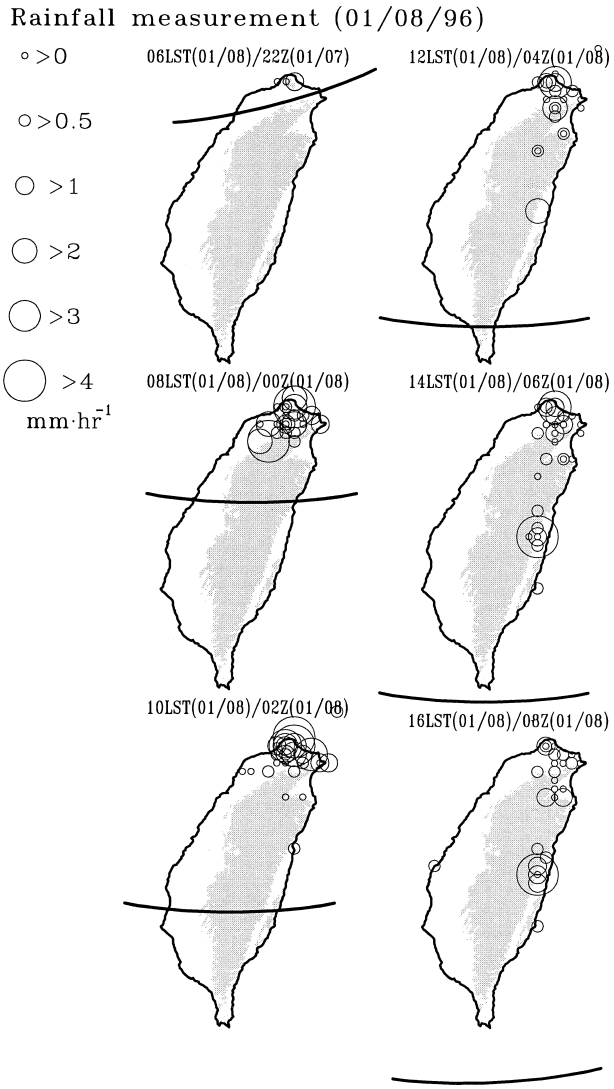

FIG. 9. Station rainfall observations over Taiwan at different local standard times; rainfall amounts are indicated by various-sized circles, while the cold front is marked by a thick dark line.

level divergent (convergent) center is situated ahead of a trough, while the reverse situation is located ahead of a ridge. Although the Hadley circulation is maintained by the north–south differential heating, it may be modulated in some way by the divergent circulation associated with the eastward-propagating synoptic disturbances in midlatitudes. It is thus of interest to explore the collaborative modulation of the two cold surge couplets on the local Hadley circulation. The examination of this impact may give an understanding to another dimension of the tropical–midlatitude interaction associated with east Asian cold surges.

Shown in Figs. 12a and 12b are divergent circulations depicted in terms of velocity potential (χ) and divergent wind (V_D) at 200 and 925 mb, respectively: (χ, V_D) (200 mb) and (χ, V_D) (925 mb). The local Hadley circulation in the south and southeast Asian sector may be inferred from the contrast of divergent circulations at these two levels. However, the detailed structure of this local circulation is better depicted by the mass flux function ψ_M[1] (120°E) (Fig. 12c). With a major upward branch in the Tropics and a major downward branch in midlatitudes, the basic structure of the local Hadley circulation resembles the one often portrayed in previous studies. In light of its link with a cold surge, the following two questions are raised:

1) How does the local Hadley circulation interact with the midlatitude synoptic disturbances associated with the cold surges presented in Fig. 3?
2) As revealed from the mass flux function ψ_M (120°E) (Fig. 12c), the local Hadley circulation exhibits a double-cell structure. The direction of the northern cell is opposite to Chu and Park's (1984) depiction; is there any dynamic implication of the difference?

The answer to the first question can be gained through a comparison between Fig. 12a and Fig. 3b. An upper-level convergent center appears ahead of both the Lake Baikal ridge (R_2) and the Japan ridge (R_1). The air exiting the upper-level divergent center south of the tropical Southeast Asian high (H) converges toward the two aforementioned synoptic convergent centers. Corresponding to these two midlatitude upper-level convergent centers, two lower-level divergent centers exist south of Lake Baikal and southeast of Japan (Fig. 12b), respectively. The former divergent center is located on

[1] Following Chen et al. (1988), the mass flux function is computed by the following integration: $\psi_M(p) = \int_o^p (\partial v_D/\partial y)\, dp$, where v_D is the meridional divergent wind averaged over a longitudinal zone between 117.5° and 122.5°.

the downstream side of the continental couplet's outflow, while the latter divergent center is situated on the downstream side of the oceanic couplet's outflow. The air mass exiting these two lower-level divergent centers forms the returning flow converging toward the elongated lower-level convergent center along the tropical trough. Evidently, the upward branch of the local Hadley circulation in the Tropics is jointly maintained by the air mass exiting the two midlatitude lower-level divergent centers and the air mass converging toward the two midlatitude upper-level convergent centers. Despite the fact that the local Hadley circulation is depicted in terms of a latitude height ψ_M cross section at a given longitude, the intensity of this local Hadley circulation is determined jointly by the mass exchange of the continental anticyclonic cell H_2 and the oceanic anticyclonic cell H_1 with the tropical trough.

Analyzing a WMONEX cold surge, Chu and Park (1984) inferred from heat and moisture transport the existence of a double-cell structure of the local Hadley circulation associated with this surge. The lower-level heat and moisture divergence in the northern part of the South China Sea led them to suggest a separation of this double-cell structure by a descending branch over this region. In contrast, it is revealed from the comparison between the upward motion along the cold front in Fig. 7a and surface pressure p_s in Fig. 6c that a convergent zone coincident with this front is in parallel with a high pressure zone ahead of the front. As argued in section 3, the advance of the continental cold surge outflow slowed down by this high pressure zone (formed by the westward extension of the oceanic anticyclone H_1) may induce the upward motion along the cold front. This argument is further strengthened by the following fact. The strong low-level divergent flows that radiate out of the divergent center adjacent to BoHai (a margin sea west of the Yellow Sea) are terminated along the cold front. It is also revealed from the comparison between Figs. 7a and 6c that the prefront high pressure zone coincides with descending motion. This juxtaposition of the convergence zone along the front and the high pressure zone ahead of the front results in the mass flux function ψ_M being convex upward in the lower troposphere in the vicinity of Taiwan. Evidently, this convergence–high surface pressure juxtaposition across the cold surge front is conducive to the formation of a double-cell structure of the local Hadley circulation. An answer to the second question can be derived from our previous arguments.

5. Impact on the surface weather conditions in Taiwan

Locations of the cold surge front estimated with the GMS IR/visible images (Fig. 2) and JMA surface charts (Fig. 5) indicate that this front arrived in Taiwan at about 2200 UTC 7 January 1996 and left the island at 0500 UTC 8 January. Regardless of the short north–south extent (~400 km), it takes about 7 h for this front to pass through this island. Since observations of high-density surface stations (Fig. 13) are available, the passage of this well-organized cold surge front gives us a unique opportunity to explore the impact of this cold surge on the surface weather conditions over Taiwan. The characteristic changes of several surface variables are examined. Our major attention is focused on the following three aspects:

1) The arrival of a cold surge is characterized by a sharp rise of p_s, sudden drop of T_s, and drastic increase of the northerlies/northeasterlies ($v_s < 0$). Are these characteristics of the cold surge arrival uniform over all stations of Taiwan from north to south?
2) It was revealed from our previous studies (Chen et al. 1998, 1999, 2000, 2001) that T_s exhibits a distinct diurnal variation, while p_s shows both diurnal and semidiurnal variations. How are diurnal variations in T_s and p_s over the entire island of Taiwan modulated by the cold surge?
3) Examining the difference of passage times between the edge of the density current and the thermal front, Chang et al. (1983) pointed out that the advance of a cold surge behaves as an extremely shallow density current. Because of the lack of observations, the vertical structure of a cold surge has still not been well explored. As mentioned previously, the horizontal dimensions of Taiwan are about 400 km (north–south) × 150 km (east–west) with the tallest mountain (Yushan) about 4000 m. The east–west slope of terrain on this island is larger than 4 km/100 km (4%). Thus, surface observations at stations with different elevations offer us an alternative way to analyze the vertical structure of a cold surge.

The first two aforementioned aspects of the cold surge are explored in terms of time series of some variables observed at all stations shown in Fig. 13 and the y–t diagram of some variables at stations along the west and east coasts from north to south. Insight into the third aspect is provided by time series of various variables from stations along the dashed line in Fig. 13.

a. Surface weather conditions

The arrival of a cold surge is determined by the following four criteria: (a) a sharp rise of p_s(≥5 mb), (b) a sudden drop of T_s(≥4°C or more), (c) a drastic increase of prevailing northerly/northeasterly winds (≥3 m s^{-1}), and (d) changes of p_s and T_s over 24 h (Δp_s and ΔT_s, respectively) larger than the amplitudes of these two variables' climatological diurnal/semidiurnal cycles in January (when diurnal variations of these two variables are completely suppressed). The first three criteria were introduced in section 1, while the fourth criterion is a new one. Observations of stations that meet different sets of criteria are marked by the following

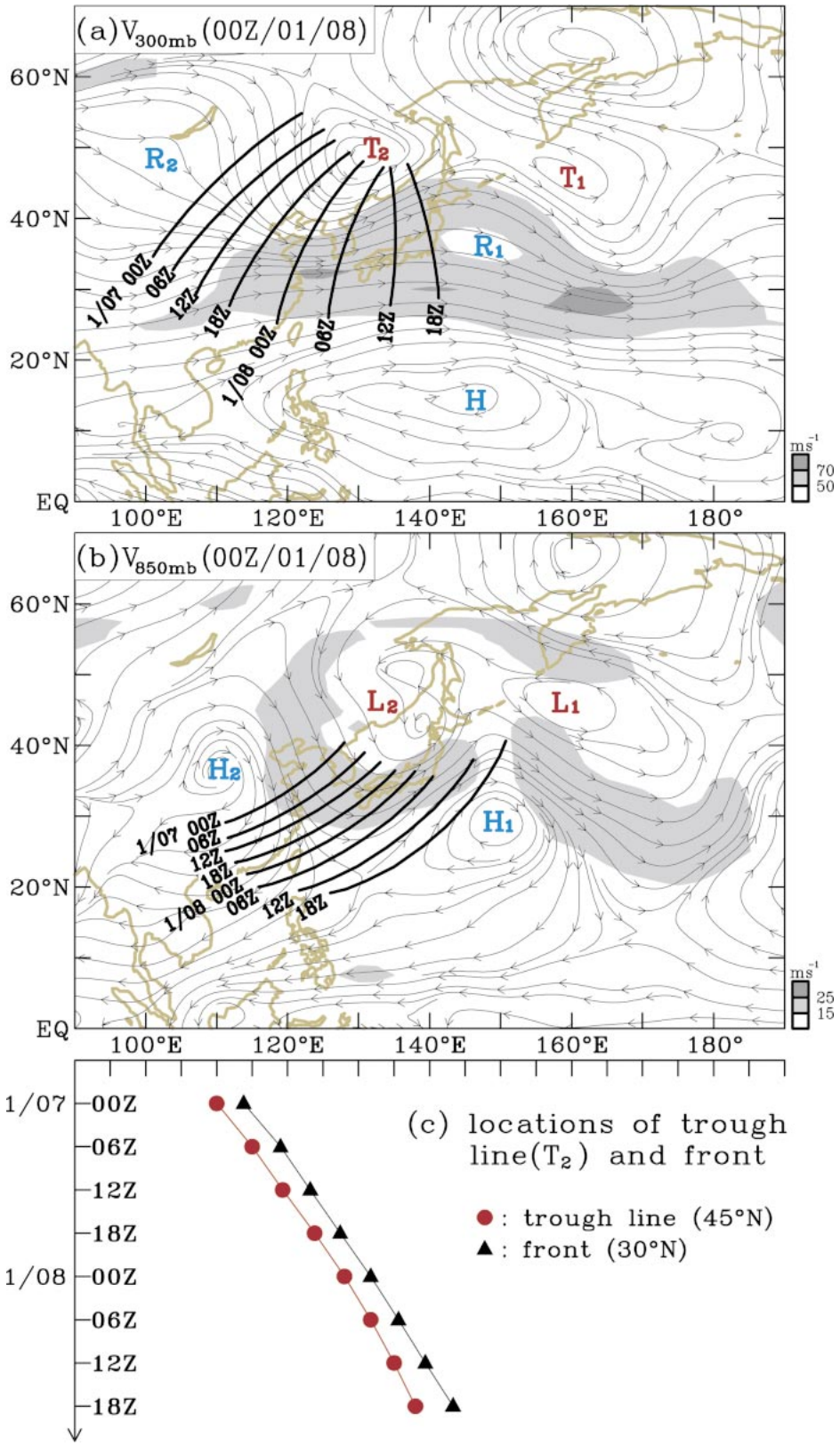
(a) V_{300mb} (00Z/01/08)
60°N
40°N
20°N
EQ
100°E
120°E
140°E
160°E
180°
R_2
T_2
T_1
R_1
H
1/07 00Z
06Z
12Z
18Z
1/08 00Z
06Z
12Z
18Z
ms⁻¹
70
50
(b) V_{850mb} (00Z/01/08)
L_2
L_1
H_2
H_1
25
15
1/07
1/08
(c) locations of trough line(T_2) and front
● : trough line (45°N)
▲ : front (30°N)

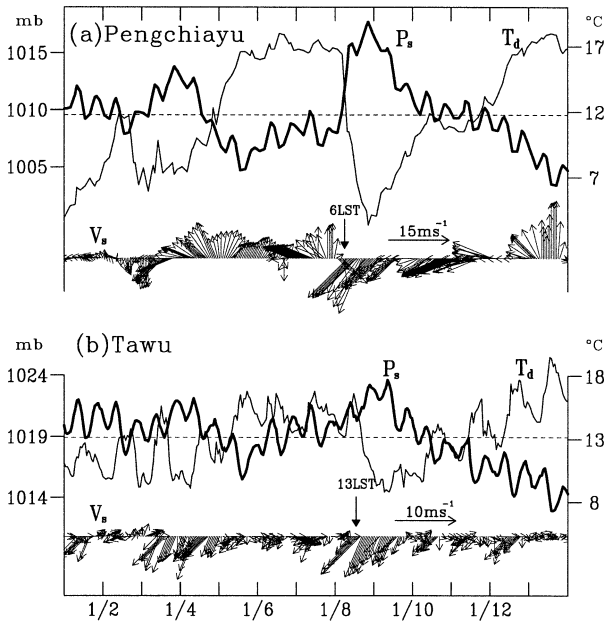

FIG. 11. Time series of surface pressure (p_s − thick solid line), surface dewpoint (T_d − thin solid line) and surface wind vector (V_s) observed at two stations: Pengchiayu (WMO-46695) and Tawu (WMO-46754). The arrival time of the cold surge is indicated by a downward vector on surface wind observations.

different symbols in Fig. 13: ○ = criteria (1, 2, 3, 4); □ = criteria (1, 2, 3) with suppressed diurnal cycle; △ = criteria (2, 3, 4); * = criteria (3, 4); and ▲ = no obvious impact.

As shown in Fig. 13, observations of all stations in northern Taiwan belong to the first group (○). With the exception of the two small island stations (Penhu and Tungchitao) west of Taiwan and the two tall mountain stations (Alishan and Yushan), the rest of the stations fall into two groups: group * in western and southern Taiwan, and group □ in eastern Taiwan. The sharp rise of p_s occurs only in northern and eastern Taiwan where diurnal variations in p_s and T_s are either completely or partly suppressed, perhaps due to dense cold air and cloudiness (as inferred from rainfall shown in Fig. 9). In western, southwestern, and southern Taiwan, the p_s jump is replaced by the existence of distinct diurnal variations in p_s and T_s. The maximum east–west extent of Taiwan is only about 150 km. It is interesting to find that the characteristics of a cold surge can exhibit such significant differences between the two sides of this island.

To further illustrate the modification of the surface weather conditions by the cold surge, the y–t diagrams of p_s, T_s, and v_s along both coasts of Taiwan are displayed in Fig. 14. The northerlies/northeasterlies of all stations along both coasts of Taiwan are marked by a blue color in Figs. 14c,f. The southward advance of the surge is clearly indicated by the onset time of strong northerlies/northeasterlies on 8 January. The advancing speed of the surge inferred from v_s is consistent with that estimated from the front location (in Fig. 2). For surface temperature, the T_s diurnal variation (Figs. 14b,e) stood out prior to and after the surge, but was almost eliminated in northern Taiwan during the surge. As indicated in Fig. 13, the T_s diurnal variation is suppressed more in southeastern Taiwan right after the surge passage. Finally, surface pressure variation over Taiwan always exhibits a semidiurnal variation caused by the westward propagation of the semidiurnal tide (Chen et al. 1998). Since the semidiurnal tide is not driven by the tropospheric forcing (Lindzen 1990), its existence is not significantly affected by the cold surge (as revealed from Figs. 14a,d). Regardless of the semidiurnal p_s variation, a sharp rise of p_s occurs over most of the east coast stations, but only in the northern part of the western Taiwan coast.

b. Vertical structure

The vertical structure of the cold surge may be inferred from observations of p_s, T_s, and v_s at stations with different elevations: Tanshui (close to mean sea level), Taichung (~100 m), Jihyuehtan (~1000 m), Alishan (~2500 m), and Yushan (~4000 m). Based on the v_s criterion, the surge can be detected at an elevation of 100 m (Taichung; Fig. 15c). Note that an arrival time difference of 3 h between Tanshui (northern Taiwan) and Taichung (central Taiwan) is due to the advance of the surge, and not elevation. The sharp rise of p_s at the arrival of a surge (Fig. 15a) may be still perceptible at Taichung (~100 m). Using the p_s and v_s criteria, one may argue that the depth of the cold surge is only on the order of 100 m. On the other hand, the sudden drop of T_s and the suppression of the T_s diurnal variation penetrate up to Jihyuehtan (~1000 m), as revealed from the T_s time series (Fig. 15b). The T_s criterion suggests that the local thermal field may be sensitive to the cold surge flow up to an elevation of 1000 m. So far, it is not indicated by any study that the cold surge flow can be this deep. One may argue that the T_s drop and the suppression of the T_s diurnal variation may be attributed to cloudiness (as inferred from Fig. 1). In addition, time series of v_s and p_s above 1000 m (Jihyuehtan) do not show coherent fluctuations with the low-level flow at Tanshui (mean sea level) and Taichung (~100 m), except in the diurnal/

←

FIG. 10. Streamline charts at 0000 UTC 8 Jan 1996 for (a) 300 mb superimposed with the 300-mb trough lines (thick solid line) at the marked synoptic times and (b) 850 mb superimposed with the cold surge front (thick solid lines) at indicated synoptic times, and (c) longitudinal locations of the trough (T_2) line at 45°N (red-dotted line) and the cold surge front at 30°N (black-triangle line) for different synoptic times. Wind speed within ranges shown in each lower-right corner are colored dark gray and gray.

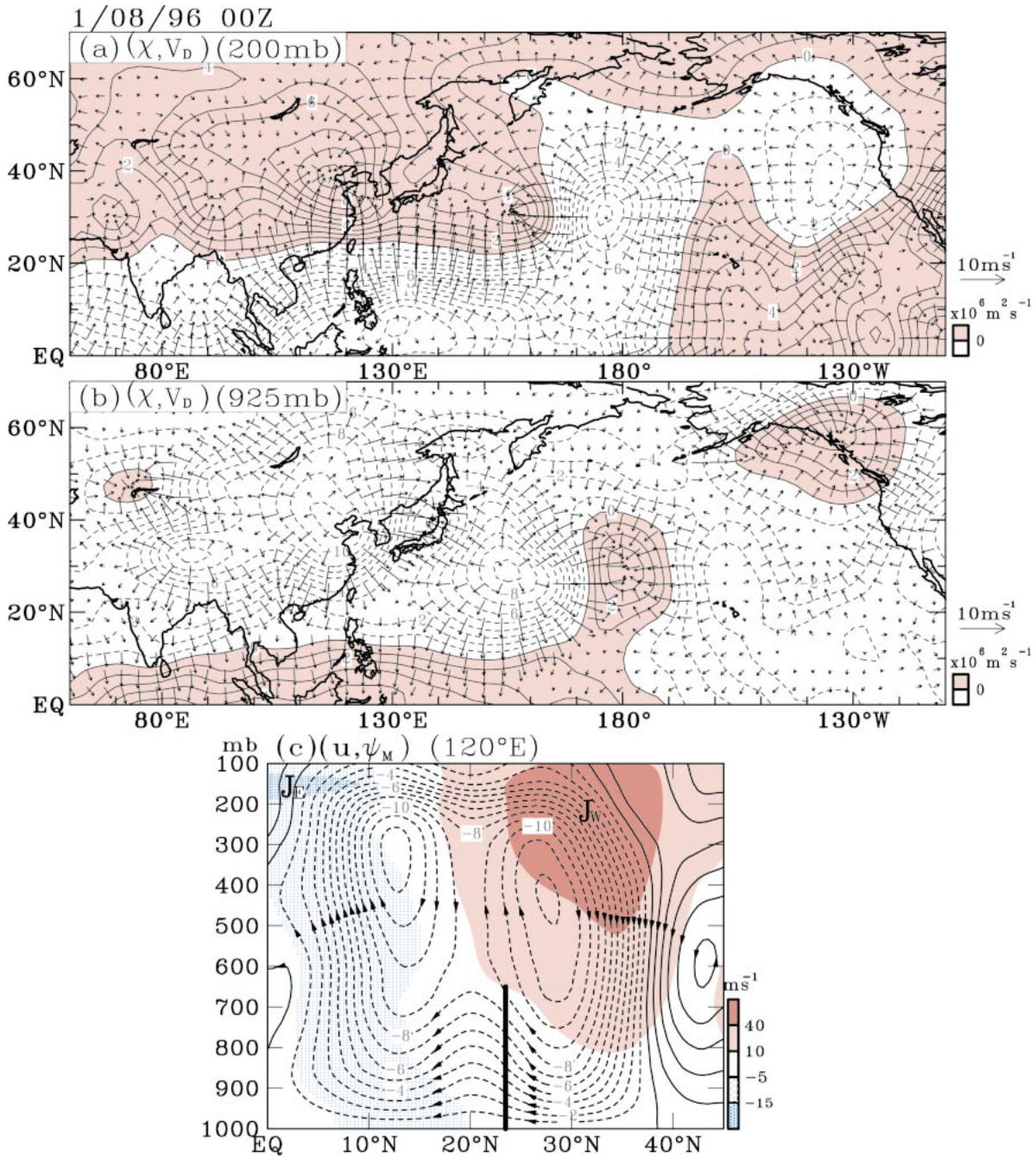

FIG. 12. Divergent circulation (χ, V_D) at (a) 200 mb and (b) 925 mb, and (c) mass flux function at 120°E, ψ_M(120°E), superimposed with zonal wind at 120°E, u(120°E). Positive values of χ(200 mb), and χ(925 mb) are colored pink. The zonal wind u(120°E) is colored according to the scale shown in the lower-right corner. Contour interval of χ(200 mb) and χ(925 mb) is 10^6 m^2 s^{-1}, while that of ψ_M(120°E) is 10^6 m^2 s^{-1}.

semidiurnal variation. Actually, the p_s time series above 1000 m are a phase ahead of these in the lower troposphere. The incoherency of p_s, T_s, and v_s time series at stations of different elevations strongly suggests that fluctuations of these variables (except diurnal/semidiurnal) are caused by different dynamic processes.

Recall that tall mountains are free of cloudiness during the passage of the cold surge front (Fig. 1). This interesting lack of clouds over Taiwan reinforces some facts derived from time series of p_s, T_s, and v_s observed at stations of various elevations: The cold surge is an extremely shallow density current. Furthermore, convection over tall mountains is suppressed by the southeast Asian high during the passage of the cold surge

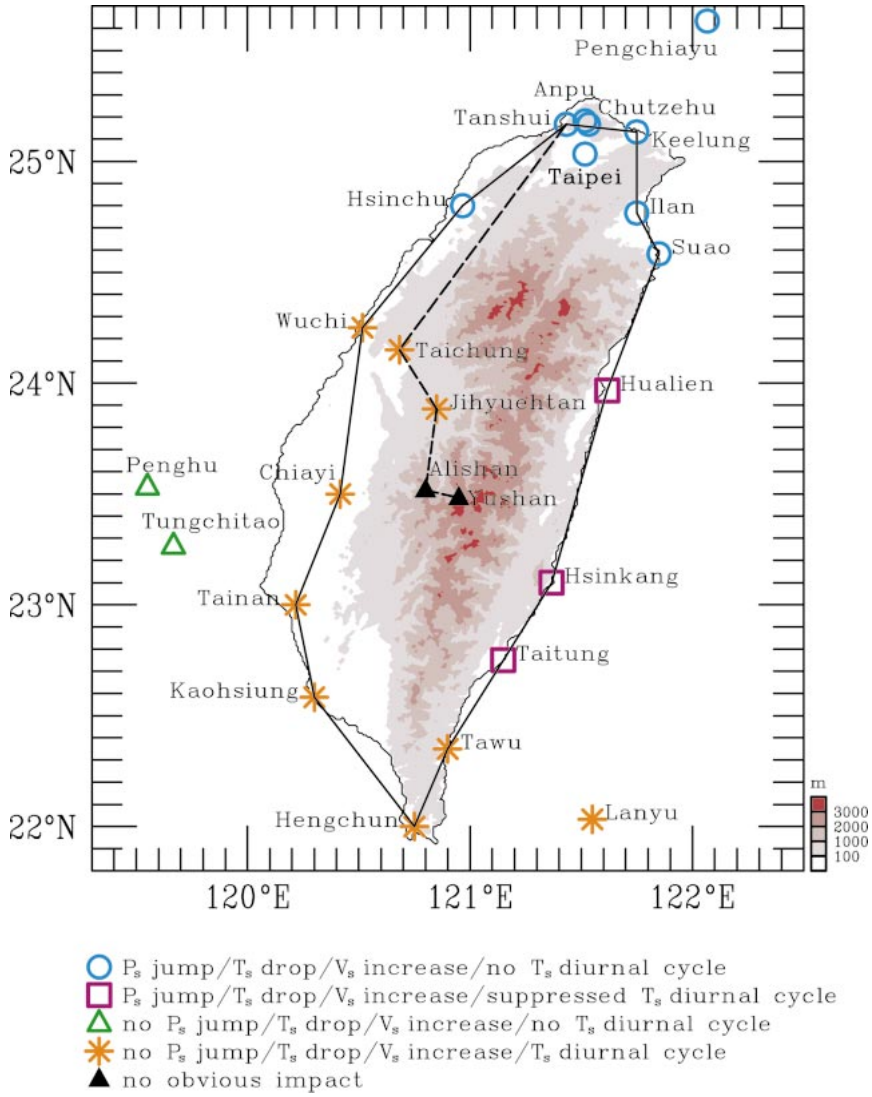

FIG. 13. Characteristics of surface meteorological variables obs during the cold surge passage at all Taiwan surface stations. Symbols are explained at the bottom.

front (further discussion concerning this argument is provided in section 5c).

c. p_s (Yushan) variation

It was suggested in section 2 that the intensification of the east Asian jet during a cold surge may follow the deepening of the upper-level short-wave trough (coupled with the cyclonic cell of the continental couplet) in northeast Asia and the amplification of the tropical southeast Asian high. This suggestion is substantiated by the correlation between variations in maximum wind speed, $|V_{\max}|_{300\text{ mb}}$ (Fig. 16a, the bottom purple line with open circles), and streamfunction gradient, $\Delta\psi_{300\text{ mb}}$ (17.5°–40°N) = $\psi_{300\text{ mb}}$(17.5°N) − $\psi_{300\text{ mb}}$(40°N) (Fig. 16a, the bottom orange line with orange triangles) at 125°E. Furthermore, the temporal variation of $\psi_{600\text{ mb}}$ (40°N) (a purple line with purple dots in the second panel from the bottom) is also shown in Fig. 16a so that we are able to explore the relationship between p_s (Yushan) and the northeast Asian trough. The coherent variations in $\psi_{600\text{ mb}}$(40°N) and maximum $|V_{\max}|_{300\text{ mb}}$ at 125°E strongly indicates that the jet intensification follows primarily the deepening of the short-wave trough. Locations of variables shown in Fig. 16a are marked in the ψ(120°E) cross section (Fig. 16b).

The surface pressure of Yushan [~4000 m indicated by a straight upward, thick solid line at (120°E, 23.5°N) in Fig. 16b], p_s (Yushan), is roughly about 640 mb, while the southeast Asian high is centered at about 17.5°N (Fig. 3). Thus, time variations in p_s (Yushan) and intensity of the southeast Asian high may be reflected by $\psi_{600\text{ mb}}$(22.5°N) and $\psi_{600\text{ mb}}$(17.5°N), respectively. Time series of these two variables (Fig. 16a) are relatively

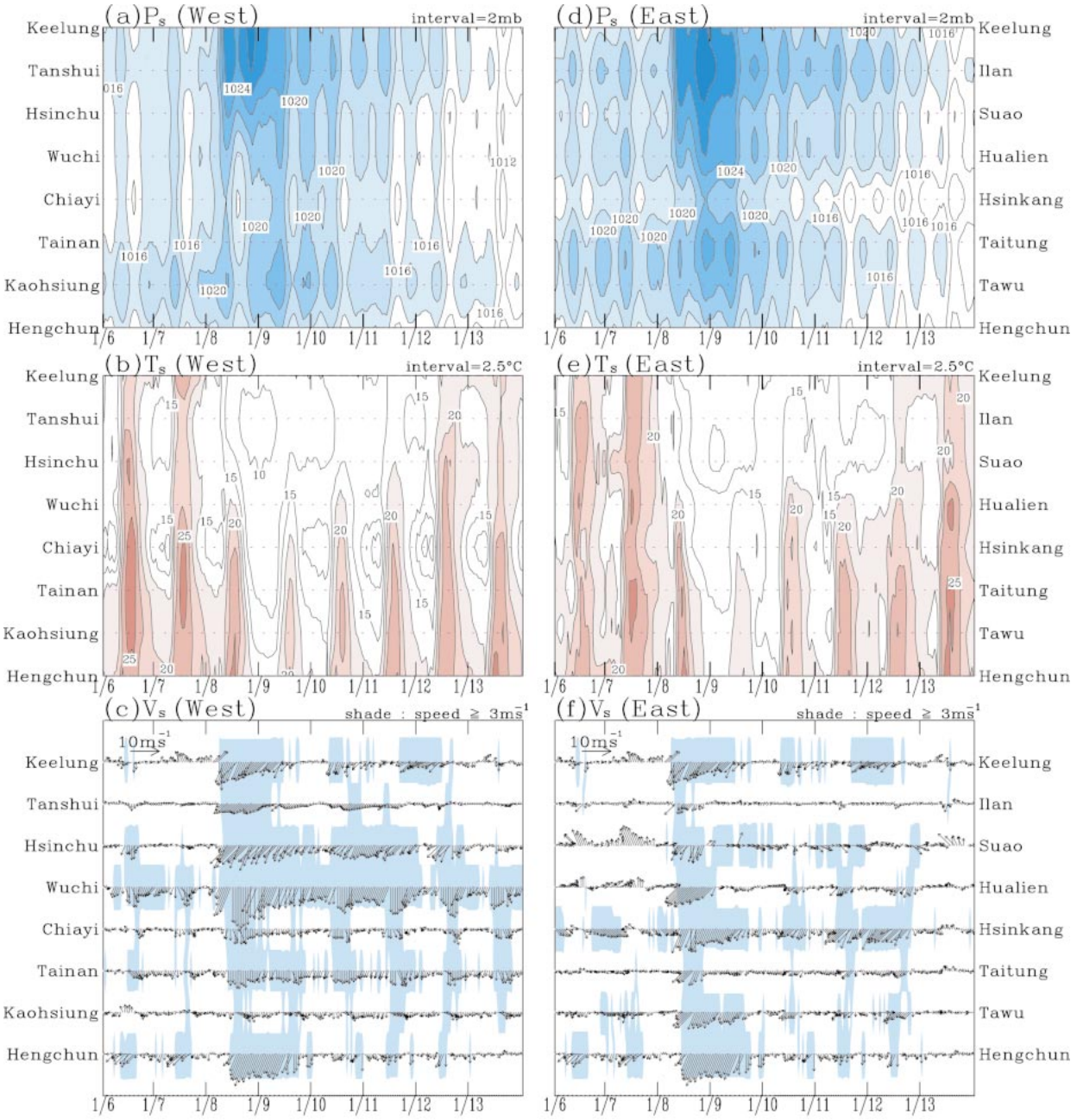

FIG. 14. The north–south–time (y–t) diagrams of station p_s, T_s, and v_s observations connected by solid lines along the west (left column) and east (right column) coast of Taiwan shown in Fig. 13. Contour intervals of p_s and T_s are 4 mb and 5°C, respectively. Surface northerlies/northeasterlies larger than 3 m s^{-1} are marked in blue.

coherent with those of p_s (Yushan). Since time variation in $\psi_{600\ \mathrm{mb}}$(40°N) at 120°E is so incoherent with that in p_s (Yushan), it becomes clear that the surface pressure at Yushan is closely modulated by the Southeast Asian high. To further support our argument, the ψ(120°E) cross section is shown in Fig. 16b. Although Yushan is located between the upper-level southeast Asian high and lower-level east Asian high, the downward extension of the former seems to affect p_s (Yushan) more effectively than the latter.

6. Concluding remarks

Prior and post-WMONEX research focused primarily on the interaction between the east Asian cold surge and the planetary-scale circulation, particularly the enhance-

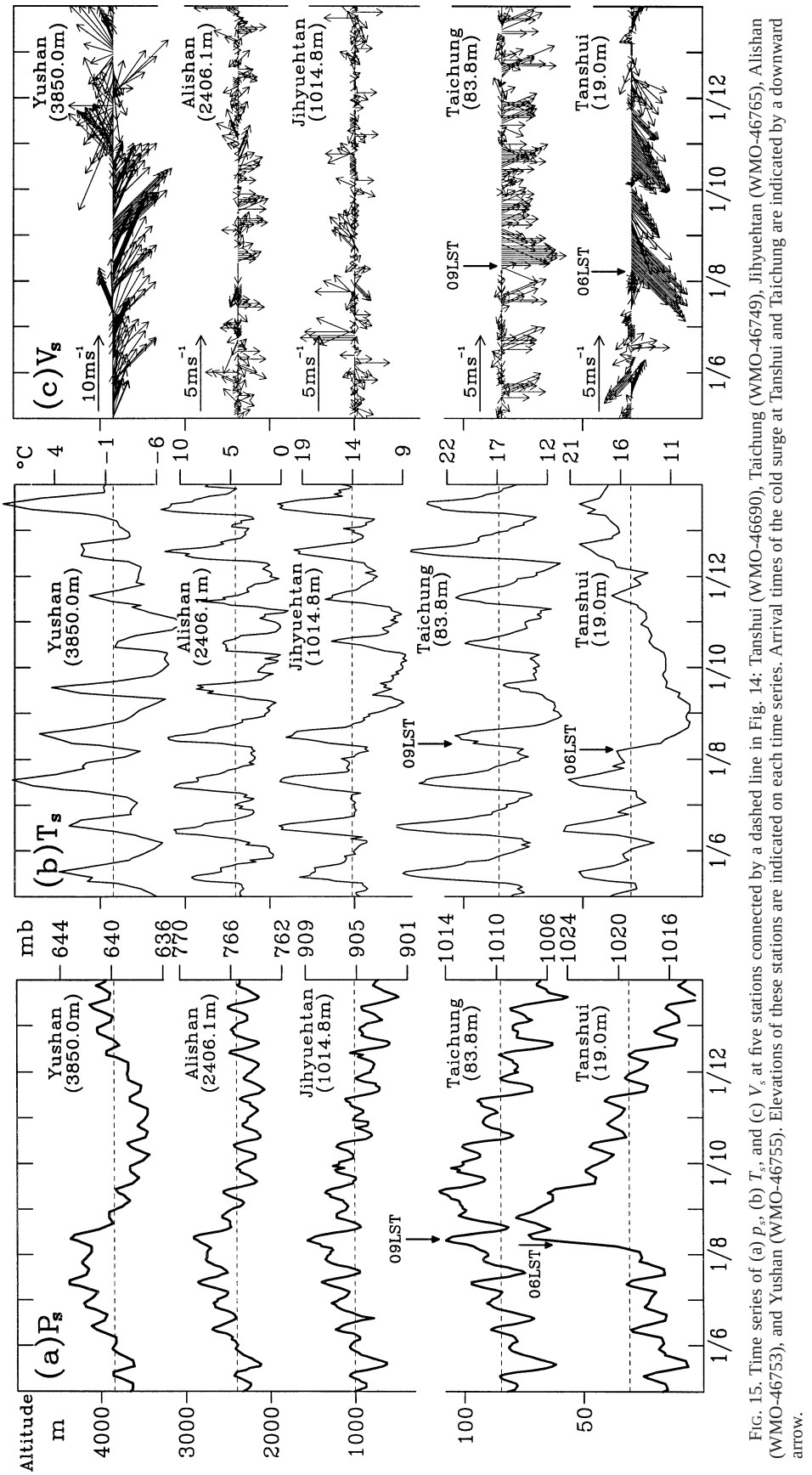

FIG. 15. Time series of (a) p_s, (b) T_s, and (c) V_s at five stations connected by a dashed line in Fig. 14: Tanshui (WMO-46690), Taichung (WMO-46749), Jihyuehtan (WMO-46765), Alishan (WMO-46753), and Yushan (WMO-46755). Elevations of these stations are indicated on each time series. Arrival times of the cold surge at Tanshui and Taichung are indicated by a downward arrow.

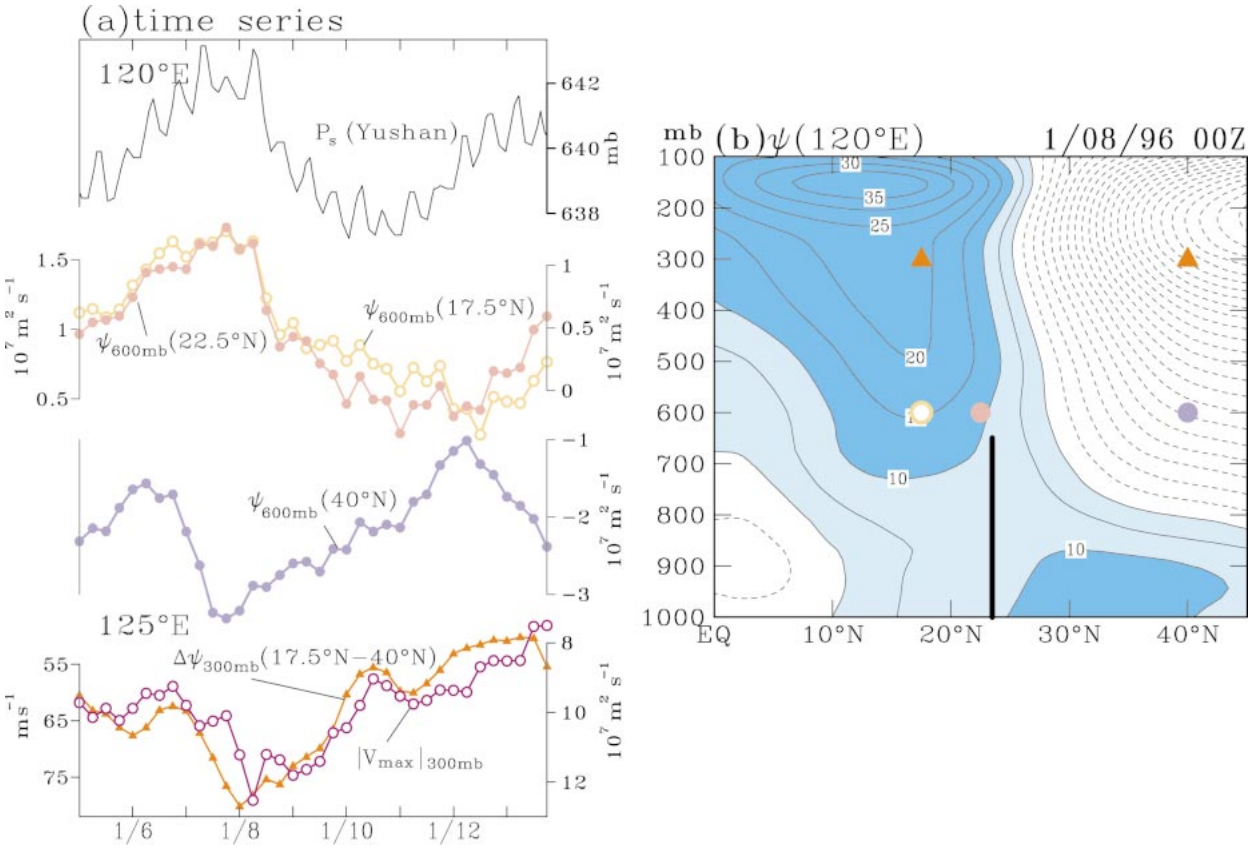

FIG. 16. (a) Time series of p_s (Yushan) and streamfunction at various points at 120°E: $\psi_{600\,mb}$ (22.5°N) (pink-dotted line), $\psi_{600\,mb}$(17.5°N) (yellow-circle line), $\psi_{600\,mb}$(40°N) (purple-dotted line), $\Delta\psi_{300\,mb}$(17.5°–40°N) streamfunction difference between 17.5° and 40°N (orange-triangle line), and 300-mb max isotach $|V_{max}|$ 300 mb at 125°E (purple open-circle line), and (b) latitude–height cross sections of streamfunction at 120°E: locations of streamfunction time series shown in (a) are marked using corresponding symbols. The location and elevation of Yushan are indicated by a vertical, thick dark line. The contour interval for ψ(120°E) is 5×10^6 m^2 s^{-1}.

ment of tropical convection, intensification of the local Hadley circulation, and speed increase of the east Asian jet caused by the cold surge (Lau and Chang 1987). However, some interesting weather features associated with cold surges need to be explored further:

- The east Asian cold surges in our case study are formed *sequentially*. How is the development of the continental cold surge upstream influenced by the aging cold surge downstream?
- How does the southeast Asian high affect in the regional winter weather in east Asia?
- What may be the impact of the cold surge on the east Asian regional weather conditions?

Perhaps, because the east-southeast Asian region consists of numerous small island countries around the East and South China Seas, the aforementioned questions did not form an urgent issue in the WMONEX. However, this situation has been reversed in the past two decades due to the population explosion and economic growth in this region. Using three cold surge criteria (Lau and Chang 1987) with the Penchiayu station observations for 11 winters (1989–2000), we identified 93 surges. Fifty-two of these surges (56%) exhibit double cold surge couplet structure. Within this group, a well-organized cold surge (with a well-defined cold front passing through Taiwan) observed by the GMS was selected as an example for us to examine the aforementioned questions with NCEP–NCAR reanalysis data, JMA surface charts, and surface observations in Taiwan. We may summarize major findings into two areas:

a. Upper-level synoptic environment

Three salient features of upper-level synoptic environment were identified. First, the couplet of this cold surge following an aging one upstream over the ocean is connected with two ridge–trough structures embedded in an upper wave train straddling the eastern seaboard of northeast Asia. Thus, during this cold surge event, the east Asian weather system is affected by both cold surge couplets. Second, the local Hadley circulation is formed not only by the divergent circulation associated with the newly developed cold surge couplet upstream, but also by that associated with the aging cold surge couplet downstream. In other words, it is formed jointly

by the lower-level divergent centers of the two cold surge couplets and the upper-level convergent centers of the two upper-trough lines in midlatitudes and the tropical upward motion over the tropical trough. Finally, the speed increase of the east Asian jet during a cold surge is more illustratively explained by the deepening of the east coast trough than the acceleration by the Coriolis force associated with the local Hadley circulation.

b. Impact on surface weather conditions

For the surface weather conditions in east Asia, the southeastward advance of the cold surge front is steered by the eastward-propagating wave train over the eastern seaboard through its coupling with the lower-tropospheric H_2/L_2 couplet of the newly formed continental cold surge. The interaction of this new cold surge couplet with the aging one exerts a significant impact on the weather development in east Asia. The warm, moist air advection by the confluent flow formed along the cold front (by both the L_2 cyclonic flow and the H_1 anticyclonic flow) assists the development of the low center (over Japan) associated with the H_2/L_2 cold surge couplet. The juxtaposition of a high pressure zone ahead of the cold surge front and the convergence zone coincident with the front facilitates the formation of a double-cell structure of the local Hadley circulation in east Asia.

Over Taiwan, clear skies over tall mountains in southern Taiwan may be a result of not only the shallowness of the cold surge, but also the suppression of convection there by the eastward-propagating southeast Asian high. Comparing the advance of the density current edge and thermal front of only the newly formed continental cold surge across Taiwan, there is no noticeable separation time as observed in previous studies. In north-northeastern Taiwan, the thermal diurnal cycle is eliminated by the cold surge wherever the sharp p_s changes occur. The depth of the cold surge defined by the p_s and v_s changes is about 100 m, while T_s changes can be seen as high as about 1000 m.

In view of these findings presented above, some dynamical implications may be drawn from the detailed analysis of the cold surge in this study. First, east Asian cold surges analyzed by previous studies were selected in terms of the $p_s - T_s - V_s$ criteria outlined by Lau and Chang (1987). However, outflows of these cold surges in east-southeast Asia may be formed by either single or double cold surge couplets. It was shown by our case study that the aging oceanic cold surge couplet may exert some impact on the newly formed continental cold surge couplet. In view of this finding, the possible effect of the aging oceanic surge couplets on the interaction of the cold surge with the planetary-scale interaction and the east Asian weather system deserves some more analysis. Second, global forecast models may not have sufficient horizontal resolution and proper physical parameterizations to portray the east Asian cold surge and its related weather phenomena. Therefore, a regional forecast model with a high resolution and versatile parameterization becomes a necessary substitute. However, a basic requirement of regional models is the proper specification of boundary conditions and proper tuning of parameterizations so that the multiple cold surge couplets and the coupled upper wave train can be fully accommodated by the model. Third, as shown by Chen (2002), interannual variations of the western tropical Pacific sea surface temperature and the cold surge vortex activity may induce a short-wave train along the North Pacific rim associated with the ENSO cycle to form an important part of global climate change. These vortices are generated by the surface northeasterly flows of multiple cold surge couplets.

The case analysis of an east Asian cold surge presented in this study not only offers us a different perspective of the possible cold surge impact on the east Asian weather system, but also reveals the quality and accessibility of the NCEP–NCAR reanalysis data and the GMS observations over this region. Through this study, it is our intent to urge the meteorological community to revive its past rigor in cold surge research.

Acknowledgments. We would like to thank Dr. G.-R. Liu, Director of the Center for Space and Remote Sensing Research, National Central University of Taiwan for offering unlimited access of the GMS data. This study is partially supported by the NSF Grants ATM-9906454 and ATM-9909650. Typing support by Mrs. Reatha Diedrichs is highly appreciated. The presentation of the paper has been greatly improved by comments and suggestions offered by two reviewers.

REFERENCES

Bluestein, H. B., 1993: Synoptic-Dynamic Meteorology in Midlatitudes. Vol. II. Oxford University Press, 594 pp.

Browning, K. A., 1990: Organization of clouds and precipitation in extratropical cyclones. *Extratropical Cyclones: The Eric Palmén Memorial Volume*, C. W. Newton and E. O. Holopainen, Eds., Amer. Meteor. Soc. 129–153.

Chang, C. P., and K.-M. Lau, 1980: Northeasterly cold surges and near-equatorial disturbances over the winter MONEX area during December 1974. Part II: Planetary-scale aspects. *Mon. Wea. Rev.*, **108,** 298–312.

——, J. E. Millard, and G. T. J. Chen, 1983: Gravitational character of cold surges during winter MONEX. *Mon. Wea. Rev.*, **111,** 293–307.

Chang, E. K. M., 1993: Downstream development of baroclinic waves as inferred from regression analysis. *J. Atmos. Sci.*, **50,** 2038–2053.

Chen, T.-C., 2002: A North Pacific short-wave train during the extreme phases of ENSO. *J. Climate*, in press.

——, and M.-C. Yen, 1999: Annual variation of surface pressure on a high east Asian mountain and its surrounding low areas. *J. Climate*, **12,** 2711–2716.

——, ——, R.-Y. Tzeng, and M.-C. Yen, 1988: Development and life cycle of the Indian monsoon: Effect of the 30–50 day oscillation. *Mon. Wea. Rev.*, **116,** 2183–2199.

——, ——, and R. Arritt, 1998: Detection of semidiurnal wind os-

cillation with a radar profiler. *Bull. Amer. Meteor. Soc.*, **79,** 1921–1924.

——, ——, and J. D. Tsay, 2000: Annual and semiannual variations of surface pressure in Taiwan. *J. Climate,* **13,** 1436–1440.

——, ——, and S. Schubert, 2001: Diurnal variation of pressure-heights: A vertical phase shift. *J. Climate,* **14,** 3793–3797.

Chu, P. S., and S. U. Park, 1984: Regional circulation characteristics associated with a cold surge event over east Asia during winter-MONEX. *Mon. Wea. Rev.,* **112,** 955–965.

Clarke, J. C., 1998: An atmospheric undular bore along the Texas coast. *Mon. Wea. Rev.,* **126,** 1098–1100.

Greenfield, R. S., and T. N. Krishnamurti, 1979: The Winter-Monsoon Experiment—Report of December 1978 field phase. *Bull. Amer. Meteor. Soc.,* **60,** 439–444.

Joung, C. H., and M. H. Hitchman, 1982: On the role of successive downstream development in east Asian polar air outbreaks. *Mon. Wea. Rev.,* **110,** 1224–1237.

Kalney, E., and Coauthors, 1996: The NCEP/NCAR 40-Year Reanalysis Project. *Bull. Amer. Meteor. Soc.,* **77,** 437–471.

Lau, K.-M., and C. P. Chang, 1987: Planetary scale aspects of the winter monsoon and atmospheric teleconnection. *Monsoon Meteorology,* C.-P. Chang and T. N. Krishnamurti, Eds., Oxford University Press, 161–202.

Lau, N.-C., and K.-M. Lau, 1984: The structure and energetics of midlatitude disturbances accompanying cold-air outbreaks over east Asia. *Mon. Wea. Rev.,* **112,** 1309–1327.

Lindzen, R. S., 1990: *Dynamics in Atmospheric Physics.* Cambridge University Press, 310 pp.

Locatelli, J. D., M. T. Stoelinga, P. V. Hobbs, and J. Johnson, 1998: Structure and evolution of an undular bore on the high plains and its effect on migrating birds. *Bull. Amer. Meteor. Soc.,* **79,** 1043–1060.

Moore, T. W., K. G. Holdsworth, and K. Alverson, 2000: Teleconnection of precipitation between east Asia and northeastern North America. *GEWEX News,* **10,** 9–12.

Orlanski, I., and E. K. M. Chang, 1993: Ageostrophic geopotential fluxes in downstream and upstream development of baroclinic waves. *J. Atmos. Sci.,* **50,** 212–225.

Palmer, T. N., and J. A. Owen, 1986: A possible relationship between some ''severe'' winters in North America and enhanced convective activity over the tropical west Pacific. *Mon. Wea. Rev.,* **114,** 648–651.

Ramage, C. S., 1971: *Monsoon Meteorology.* Academic Press, 296 pp.

Susskind, J., P. Piraino, L. Rokke, L. Iredell, and A. Mehta, 1997: Characterisics of the TOVS Pathfinder A Dataset. *Bull. Amer. Meteor. Soc.,* **78,** 1446–1472.